ЖУРНАЛ СТРУКТУРНОЙ ХИМИИ

2015. Том 56, № 7 *Декабрь* *С. 1312 – 1317*

UDC 541.6:547.53

CRYSTAL STRUCTURE, DFT STUDY, AND HIRSHFELD SURFACE ANALYSIS OF ETHYL 5-(3,4-DIMETHOXYPHENYL)-7-METHYL-3-PHENYL-5*H*-THIAZOLO[3,2-a]PYRIMIDINE-6-CARBOXYLATE

A.V. Shelke[1], N.N. Karade[1], P.Kr. Dutta[2], S.P. Bahekar[3], H.S. Chandak[3]

[1]*Department of Chemistry, Rashtrasant Tukadoji Maharaj Nagpur University, Nagpur, Maharashtra, India*
E-mail: nnkarade@gmail.com (N. Karade)
[2]*Department of Chemical Sciences, Indian Institute of Science, Education and Research (IISER) Kolkata, Mohanpur, India*
[3]*Department of Chemistry, G. S. Science, Arts and Commerce College, Khamgaon, India*
E-mail: chemants@gmail.com (H.S. Chandak)

Received November, 18, 2014

The structural characterization of fused thiazolopyrimidine **1** ($C_{24}H_{24}N_2O_4S$) is performed using the single crystal X-ray study, the DFT calculation, and the Hirshfeld surface analysis. The molecular packing of the crystal is mainly stabilized by C—H…O and C—H…π interactions. A DFT calculated HOMO-LUMO energy gap of 3.90 eV indicates a high kinetic stability of the compound. The 3D Hirshfeld surfaces and the associated 2D fingerprint plots are investigated for short contact interactions. The relative contribution of different interactions to the Hirshfeld surface indicates that the H…H, C…H, and O…H contacts account for about 83.4 % of the total Hirshfeld surface area.

DOI: 10.15372/JSC20150703

K e y w o r d s: thiazolo[3,2-a]pyrimidine, single crystal X-ray diffraction (SCXRD), DFT calculation, Hirshfeld surface analysis.

INTRODUCTION

The remarkable biological activities of fused pyrimidines which give rise to antiviral, anticancer, anti-inflammatory, and antihypertensive actions [1, 2] continue to bring this class of heterocyclic compounds to the forefront of interest and study. Thiazolo[3,2-*a*]pyrimidines are known to possess anti HSV-1 [3], anti-tumour [4], and anti-microbial activities [5] and to be CDC25B phosphatase inhibitors [6]. They also serve as diacylglycerol (DG) kinase inhibitors, calcium antagonists, group 2 metabotropic glutamate receptor antagonists, and HIV-1 reverse transcriptase inhibitors [7]. Furthermore, some thiazolo[3,2-a]pyrimidines have been assigned as new acetylcholinesterase (AChE) inhibitors, especially for the treatment of Alzheimer′s disease [8]. The molecular self-assembly through weak non-covalent forces is an important feature of biologically active systems. Among the various non-covalent forces, the hydrogen bonding [9, 10] and C—H…π [11] interactions have been widely utilized in directing the molecular self-assembly for the construction of various molecular architectures.

The single crystal X-ray diffraction (SCXRD) technique is a valuable tool in the structure-based drug design approaches during drug discovery stages [12]. However, it is to be coupled with quantum chemical calculations for the better design of physically and bio-pharmaceutically relevant crystalline

materials. In the framework of the density functional theory (DFT) approach the B3LYP hybrid functional [13] is one of the most preferred since it proved its ability of reproducing various molecular properties. The combined use of the B3LYP functional and the standard split valence basis set 6-31G(*d*) is good enough for calculating the molecular geometry [14] and vibrational spectra of large and medium size molecules [15—17]. In addition to these, the Hirshfeld surface and its 2D fingerprint plot constitute a powerful resource for visualising, exploring, analysing, and quantifying intermolecular interactions in molecular crystals with unprecedented ease and rapidity [18]. The use of SCXRD, a DFT study, and the Hirshfeld surface analysis in combination constitute a powerful tool for studying different molecular interactions and predicting their electronic properties [19]. Recently, Bedi *et al.* utilized these tools to study the effect of S…π and Se…π interactions on the packing pattern in the case of phenyl-capped cyclopenta[*c*]chalcogeneophenes [20].

We report here the crystal structure, the DFT study, and the Hirshfeld surface analysis of ethyl 5-(3,4-dimethoxyphenyl)-7-methyl-3-phenyl-5*H*-thiazolo[3,2-a]pyrimidine-6-carboxylate (**1**).

EXPERIMENTAL AND COMPUTATIONAL METHODS

The synthesis of thiazolo[3,2-a]pyrimidine was achieved by the reaction of 4-aryl-3,4-dihydropyrimidin-2(1*H*)-thione and phenyl(phenylethyny1)iodonium tosylate in K_2CO_3 as a base in the THF medium (Scheme 1) [21]. The compound was recrystallized by slow evaporation of a petroleum ether-ethyl acetate solution (3:1) yielding light yellow single crystals suitable for X-ray diffraction.

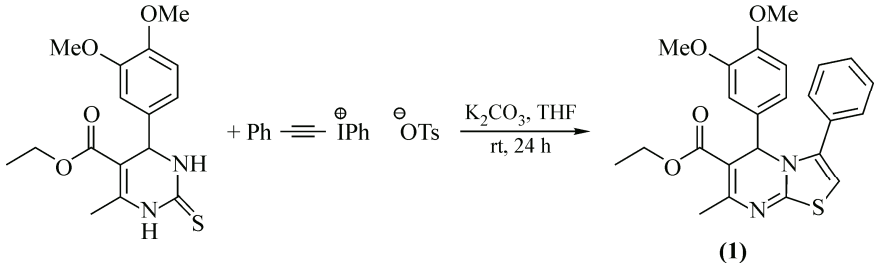

Scheme 1. Synthesis of thiazolo[3,2-a]pyrimidines

X-ray data were collected on a Bruker *SMART* diffractometer using graphite-monochromated MoK_α (k = 0.71073 Å) radiation at 293(2) K. The structure was solved by direct methods using the SHELXS97 software [22]. All of the non-hydrogen atoms were refined anisotropically by full-matrix least-squares on F^2 using SHELXL97. All H atoms were allowed to ride on the parent atom in the model during the refinement. An absorption correction was performed using SADABS [23]. The CIF file containing complete information on the studied structure was deposited with CCDC, deposition number 948903, and is freely available upon request from the following web site: www.ccdc.cam.ac.uk/data_request/ci. The crystallographic data for the titled compound are summarised in Table 1.

A density functional theory (DFT) calculation using the GAUSSIAN-09 program package [24] and employing the hybrid [25, 26] Becke three-parameter exchange density functional with the LYP correlation functional (B3LYP) [27] and the 6-31G(*d*) basis set was performed on the titled molecule. Starting geometries were taken from the single crystal X-ray data. The DFT optimised structure is compared to the single crystal X-ray structure. A comparison of the selected bond distances and angles of **1** obtained from the crystal structure analysis and the DFT calculation is given in Table 2. Hirshfeld surface analyses were carried out and finger print plots were plotted using CRYSTAL EXPLORER [28]. The normalized contact distance (d_{norm}) displays surface with a grey—white—black color scheme, where dark black spots highlight shorter contacts, white areas represent contacts around the van der Waals separation and black regions are devoid of close contacts. Electrostatic potentials were calculated using the TONTO [29, 30] computer program integrated to CRYSTAL EXPLORER. Crystal geometry was used as input to TONTO.

Table 1

Crystal and experimental data on **1** (CCDC948903)

Formula	$C_{24}H_{24}N_2O_4S$
Formula weight	436.52
Crystal color, habit	Light yellow, Block
Crystal size, mm	0.42×0.21×0.20
Crystal system	Triclinic
Space group	*P*-1
Temperature, K	298
Unit cell dimension: *a*, *b*, *c*, Å; α, β, γ, deg.	10.480(2), 11.164(2), 11.328(2); 64.887(4), 65.187(4), 87.235(3)
V, Å^3	1075.6(3)
Calculated density, Mg/m^3	1.348
No. of reflections [$I > 2\sigma(I)$]	3423
Z	2
Absorption coefficient *F*(000)	460
θ range for data collection	2.0—26.1
Index ranges	$-12 \le h \le 11$, $-13 \le k \le 13$, $-13 \le l \le 13$
Refinement method	Full-matrix least-squares on F^2
Data / restraints / parameters	4037 / 0 / 284
Calculated weights, *w*	$1/[\sigma^2(F_0^2) + (0.0916P)^2 + 0.427P]$, where $P = (F_0^2 + 2F_c^2)/3$
Goodness-of-fit on F^2	1.12
Final *R* indices [$I \ge 2\sigma(I)$]	$R_1 = 0.036$, $wR_2 = 0.165$
$(\Delta/\sigma)_{max}$	< 0.001
$\Delta\rho_{max}$ / $\Delta\rho_{min}$, e/Å^3	0.44 / –0.65

Table 2

Selected geometrical parameters and DFT *calculations* (Å, deg.)

Bond lengths	X-ray	DFT	Bond angles	X-ray	DFT	Bond angles	X-ray	DFT
N1—C9	1.356(3)	1.371	C9—N1—C12	118.89(17)	117.96	C11—C12—C13	113.29(16)	114.12
N1—C12	1.487(2)	1.489	C7—N1—C12	124.81(16)	124.95	N2—C9—S1	122.22(16)	122.78
N2—C9	1.303(3)	1.300	C9—N2—C10	115.74(18)	116.61	N1—C9—S1	109.80(15)	110.20
N2—C10	1.390(3)	1.387	C11—C10—N2	122.18(19)	121.88	C8—S1—C9	90.94(10)	90.28
C10—C11	1.365(3)	1.374	N2—C9—N1	128.0(2)	127.02	C9—N1—C7	114.68(17)	114.57
C10—C24	1.498(3)	1.510	C10—C11—C21	128.03(19)	127.39	C7—C8—S1	112.54(18)	112.45
C11—C21	1.461(3)	1.465	C10—C11—C12	121.48(18)	120.63	C8—C7—N1	112.04(19)	112.50
C12—C11	1.522(3)	1.527	N1—C12—C11	108.01(15)	107.69	C8—C7—C6	126.0(2)	125.22
S1—C8	1.729(2)	1.754	N1—C12—C13	111.33(15)	111.52	N1—C7—C6	121.97(18)	122.23
S1—C9	1.742(2)	1.765						
N1—C7	1.407(3)	1.406						
C7—C8	1.336(3)	1.354						

RESULTS AND DISCUSSION

Compound **1** crystallizes in the triclinic (*P*-1) space group with cell parameters *a* = 10.480(2) Å, *b* = 11.164(2) Å, *c* = 11.328(2) Å. The molecular structure of compound **1** is built up from two fused five- and six-membered rings linked to methyl, phenyl, and ethylcarboxylate groups as shown in Fig. 1.

The crystal structure shows that the fused thiazole and pyrimidine rings are nearly in the same plane except the sp^3 hybridized carbon atom (C12). The ring puckering parameters (Cremer and Pople, 1975) [31] for the pyrimidine ring are $q_2 = 0.2279$ Å, $q_3 = -0.0879$ Å, $Q = 0.2443$ Å; $\theta = 111.09°$ and $\varphi = 132.82°$. The selected geometrical parameters are given in Table 2.

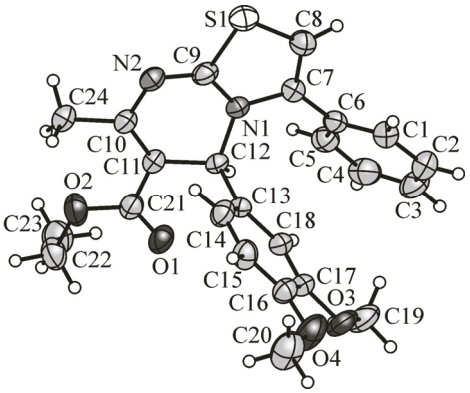

Fig. 1. Molecular structure of the titled compound with displacement ellipsoids drawn at the 50 % probability level

The molecules pack in a stacking-like mode, arranged in an alternating pattern diagonally across the *ab* plane of the unit cell. The molecular packing of the crystal is mainly stabilized by C—H…O and C—H…π intermolecular interactions. The distance between the sp^2 oxygen and aromatic hydrogen atoms (C—H···O) is 2.658 Å (the sum of the van der Waals radii is 2.72 Å). The C—H…π distances (C—H(23B)…C(5) and C—H(23C)…C(3)) are 2.863 Å and 2.870 Å (Fig. 2).

Compound **1** was optimized at the B3LYP/6-31G(*d*) level. The bond lengths and bond angles of the optimized structure of **1** are listed in Table 2. The bond distances of the optimized structure of **1** are found slightly longer than those obtained in the single crystal X-ray structure, except N2—C9, N2—C10, and N1—C7 which are slightly shorter (≈0.01 Å). All bond angles involving pyrimidine nitrogen atoms in the DFT optimized geometry are slightly shorter that those determined experimentally, except C9—N2—C10. These tiny differences between the calculated and observed geometries could be attributed to the crystal packing of the molecules in the solid state.

The calculated HOMO-LUMO gap of molecule is 3.90 eV, which shows a high kinetic stability of the structural system. The molecular orbital pictures of HOMO and LUMO are depicted in Fig. 3. The electron density of HOMO is located on fused thiazolopyrimidine and phenyl rings attached to the pyrimidine ring while in LUMO it is mostly located on fused thiazolopyrimidine rings.

The calculated vibrational spectrum has no imaginary frequencies, implying that the optimised geometry is located at the minimum point of the potential surface. Some selected experimental and calculated IR frequencies are given in Table 3. The close resemblance in these frequencies could be interpreted as the convenience and suitability of the utilized computational approach.

The Hirshfeld surfaces of **1** are illustrated in Fig. 4 showing the surfaces that have been mapped over d_{norm}. The black pointed spots are due to C—H…O interactions, white spots are due to C—H…π interactions and other visible spots on the surface correspond to H…H contacts. The contribution of intermolecular contacts to the Hirshfeld surfaces are H…H (52.1 %), C…H (17 %), O…H (14.3 %), and others (16.6 %). The O…H/H…O intermolecular contacts appear as two wings in the 2D fingerprint plots (Fig. 5). At the top left and bottom right of the fingerprint plot there are characteristic ″wings″ which are identified as a result of C—H…π interactions [32, 33].

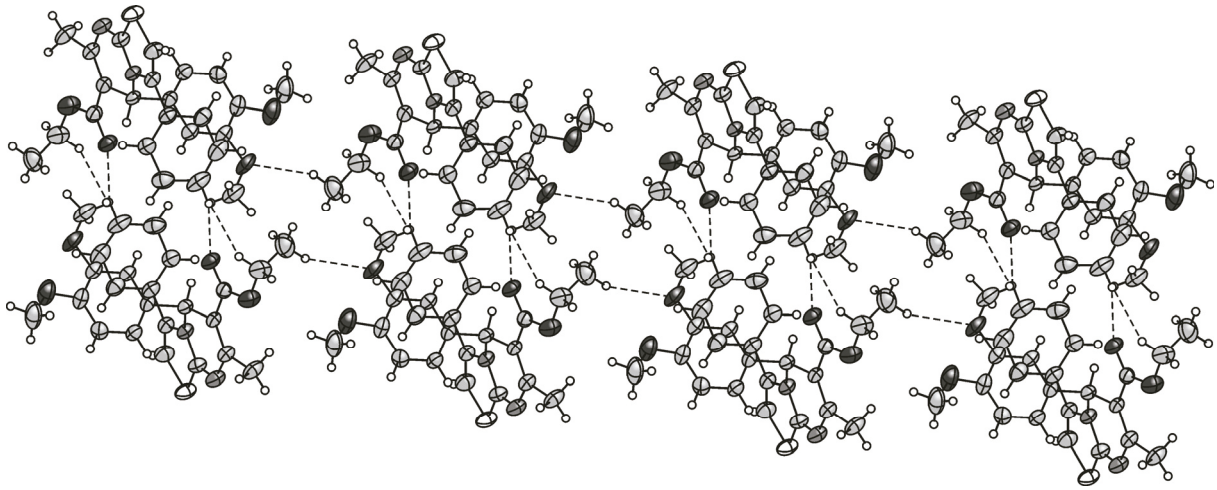

Fig. 2. Packing diagram of compound **1** showing intermolecular non-bonding interactions *via* C—H…O and C—H…π

Table 3

Selected experimental and calculated vibrational frequencies of **1**

Exp. Freq., cm^{-1}	Calc. Freq., cm^{-1}	Assignment	Exp. Freq., cm^{-1}	Calc. Freq., cm^{-1}	Assignment
1558.46	1558	C=C str + C=N str + C—C—H bend	1092.26	1114	C—O str + C—H bend
1271.92	1276	C—C—O bend + C—N str	1578.55	1572	C=C str
1365.37	1366	C—N str	1271.92	1282	ArC—O str
1737.39	1740	C=O str	1313.64	1308	C=C str + C—H bend
1130.49	1139	C—N str + C—H bend	1339.43	1340	C—N str

The electrostatic potential is mapped on the Hirshfeld surface using the STO-3G basis set at the Hartree-Fock theory level over the range of ±0.01 a.u. (Fig. 6). The positive electrostatic potential (black region) over the surface indicates hydrogen donor potential, whereas the hydrogen bond acceptors are represented by the negative electrostatic potential (grey region) [17].

CONCLUSIONS

To summarize, we have reported the crystal and electronic structure evaluation using the DFT and Hirshfeld surface analyses of compound **1** ($C_{24}H_{24}N_2O_4S$). In this compound, the fused thiazole and pyrimidine rings are nearly in the same plane, except the sp^3 hybridized carbon atom (C12). The molecular packing of the crystal is mainly stabilized by C—H···O and C—H…π interactions. The comparison of the solid state and the optimized geometries shows a few minor structural differences and the overall conformation is the same in both cases. The DFT calculated bond lengths and harmonic vibrations were obtained in very good agreement with the available experimental data. An examina-

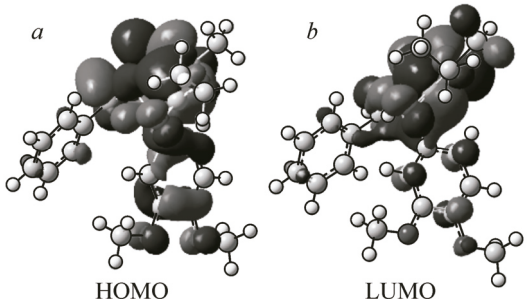

Fig. 3. Molecular orbital pictures of HOMO-LUMO

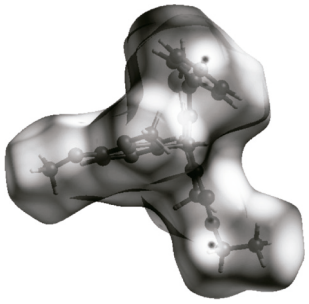

Fig. 4. d_{norm} mapped on the Hirshfeld surface for visualizing the molecular intercontacts of **1**

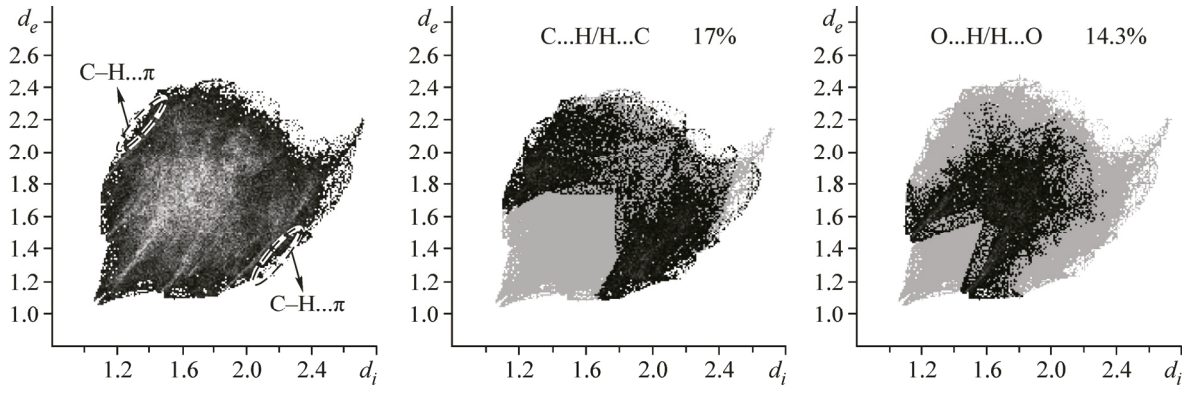

Fig. 5. Fingerprint plot of **1**: full and resolved into C…H and O…H contacts showing the percentages of contacts contributed to the total Hirshfeld surface area of the molecule

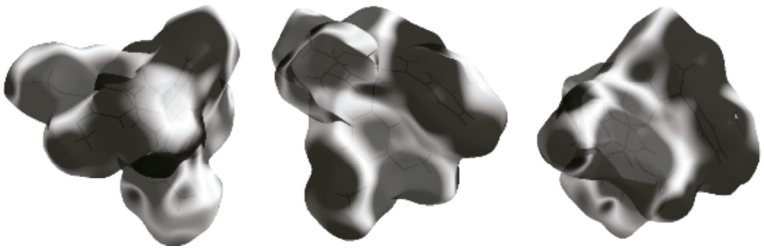

Fig. 6. Electrostatic potential mapped on the Hirshfeld surface (different orientation) within ±0.01 a.u.
Black region corresponds to the positive electrostatic potential and grey region to negative electrostatic potential

tion of close intermolecular interactions using the Hirshfeld surfaces and the associated 2D fingerprint plots revealed that the H…H, C…H, and O…H contacts account for about 83.4 % of the total Hirshfeld surface area. All these results could be useful to the chemists to study thiazolopyrimidine and develop its new analogues as potential drugs.

We thank Dr. Sanjio Zade, IISER Kolkata for many helpful discussions and for his valuable comments on the manuscript. N.N. Karade is thankful to the Department of Science and Technology, New Delhi, India (No. SR/S1/OC-72/2009) for financial support. H.S. Chandak is thankful to UGC, New Delhi, India (No. F. No. 41-335/2012) for financial support.

REFERENCES

1. *Rovnyak G.C., Kimbali S.D., Beyer B.G. et al.* // J. Med. Chem. – 1995. – **38**. – P. 119 – 129.
2. *Kappe C.O.* // Eur. J. Med. Chem. – 2000. – **35**. – P. 1043 – 1052.
3. *Mohamed S.F., Flefel E.M., Amr A., Abd EI-Shafy D.N.* // J. Med. Chem. – 2010. – **45**. – P. 1494 – 1501.
4. *Abu-Hashem A.A., Youssef M.M., Hussein H.A.R.* // J. Chin. Chem. Soc. – 2011. – **58**. – P. 41 – 48.
5. *Bekhit A.A., Fahmy H.T.Y., Rostom S.A.F., Baraka A.M.* // Eur. J. Med. Chem. – 2003. – **38**. – P. 27 – 36.
6. *Kolb S., Mondésert O., Goddard M.L. et al.* // Chem. Med. Chem. – 2009. – **4**. – P. 633 – 648.
7. *Pan B., Huang R., Zheng L. et al.* // Eur. J. Med. Chem. – 2011. – **46**. – P. 819.
8. *Zhi H., Chen L.M., Zhang L.L. et al.* // ARKIVOC. – 2008. – **13**. – P. 266 – 277.
9. *Desiraju G.R., Steiner T.* The Weak Hydrogen Bond in Structural Chemistry and Biology. – Oxford: Oxford University Press, 1999.
10. *Zhang Y., Yang Z., Yuan F. et al.* // J. Am. Chem. Soc. – 2004. – **126**. – P. 15028.
11. *Schneider H.J.* // Angew. Chem. Int. Ed. – 2009. – **48**. – P. 3924.
12. *Baias M., Pırnau A., Chis V. et al.* // J. Optoelectron. Adv. Mater. – 2006. – **8**. – P. 205 – 207.
13. *Becke A.D.* // J. Chem. Phys. – 1993. – **98**. – P. 5648 – 5652.
14. *Chandak H.S., Zade S.S.* // Organic Electronics. – 2014. – **15**. – P. 2184 – 2193.
15. *Korth H.G., de Heer M.I., Mulder P.* // J. Phys. Chem. – 2002. – **106**. – P. 8779.
16. *Zhu W.L., Puah C.M. et al.* // J. Mol. Struct. (Theochem). – 2000. – **528**. – P. 193 – 198.
17. *Chis V.* // Chem. Phys. – 2004. – **300**. – P. 1.
18. *Spackman M.A., Jayatilaka D.* // Cryst. Eng. Comm. – 2009. – **11**. – P. 19 – 32.
19. *Seth S.K., Saha N.C., Ghosh S., Kar T.* // Chem. Phys. Lett. – 2011. – **506**. – P. 309 – 314.
20. *Bedi A., Debnath S., Chandak H.S., Zade S.S.* // RSC Adv. – 2014. – **4**. – P. 35653 – 35658.
21. *Shelke A.V., Bhong B.Y., Karade N.N.* // Tetrahedron Lett. – 2013. – **54**. – P. 600 – 603.
22. *Sheldrick G.M.* // Acta Crystallogr. A. – 2008. – **64**. – P. 112 – 122.
23. *Bruker S.* SADABS. Bruker AXS, Madison, 2004.
24. *Frisch M.J., Trucks G.W., Schlegel H.B., Scuseria G.E. et al.* Gaussian 09, Revision C.01, Gaussian, Inc., Wallingford, CT, 2010.
25. *Parr R.G., Yang W.* Density-Functional Theory of Atoms and Molecules. – New York: Oxford University Press, 1989.
26. *Koch W., Holthausen M.C.* A Chemist′s Guide to Density Functional Theory, Wiley-VCH, Weinheim, 2000.
27. *Lee C., Yang W., Parr R.G.* // Phys. Rev. B. – 1988. – **37**. – P. 785.
28. *Wolff S.K., Grimwood D.J., McKinnon J.J., Jayatilaka D., Spackman M.A.* Crystal Explorer 3.1. – University of Western Australia, Perth, Australia, 2007.
29. *Jayatilaka D., Grimwood D.J., Lee A.A. et al.* TONTO-A System for Computational Chemistry, 2005.
30. *Spackmann M.A., McKinnon J.J., Jayatilaka D.* // Cryst. Eng. Comm. – 2008. – **10**. – P. 377 – 388.
31. *Cremer D., Pople J.A.* // J. Am. Chem. Soc. – 1975. – **97**. – P. 1354 – 1358.
32. *Spackman M.A., Byrom P.G.* // Chem. Phys. Lett. – 1997. – **267**. – P. 215.
33. *McKinnon J.J., Spackman M.A., Mitchell A.S.* // Acta Crystallogr. B. – 2004. – **60**. – P. 627.